Experimental phase diagram of zero-bias conductance peaks in superconductor/semiconductor nanowire devices

Jun Chen, Peng Yu, John Stenger, Moïra Hocevar, Diana Car, S.R. Plissard, Erik P.A.M. Bakkers, Tudor Stanescu, Sergey Frolov

Experimental phase diagram of zero-bias conductance peaks in superconductor/semiconductor nanowire devices

Jun Chen,[1]*† Peng Yu,[1]* John Stenger,[2] Moïra Hocevar,[3] Diana Car,[4] Sébastien R. Plissard,[5] Erik P. A. M. Bakkers,[4,6] Tudor D. Stanescu,[2‡] Sergey M. Frolov[1§]

Topological superconductivity is an exotic state of matter characterized by spinless p-wave Cooper pairing of electrons and by Majorana zero modes at the edges. The first signature of topological superconductivity is a robust zero-bias peak in tunneling conductance. We perform tunneling experiments on semiconductor nanowires (InSb) coupled to superconductors (NbTiN) and establish the zero-bias peak phase in the space of gate voltage and external magnetic field. Our findings are consistent with calculations for a finite-length topological nanowire and provide means for Majorana manipulation as required for braiding and topological quantum bits.

INTRODUCTION

In one-dimensional topological superconductors, zero-energy Majorana states are bound to the ends of quantum wires (1). Majorana bound states (MBSs) are predicted to disobey Abelian exchange rules, which otherwise describe all known bosonic and fermionic excitations. This can be leveraged for fault-tolerant quantum computation that proceeds via pairwise exchange of MBSs, also known as braiding (2–4). Future braiding experiments must be able to reliably generate, fuse, and move multiple MBSs (5, 6). These operations can be achieved by tuning the segments of nanowires in and out of the topological phase. To this end, we establish the boundaries of the zero-bias peak (ZBP) phase in the space of experimentally accessible parameters, namely the chemical potential and Zeeman energy. The phase diagram obtained this way is a portal into the unexplored physics of bulk topological superconductivity. It can be used to uncover the effects of electron-electron interactions (7), gauge fields (8), finite size effects, and disorder (9–13).

RESULTS AND DISCUSSION

We use a prescription for MBSs that includes the following ingredients: a one-dimensional quantum wire with spin-orbit interaction and induced superconductivity under external magnetic field B (14, 15). The right combination of these ingredients induces a topological superconductor when the following condition is satisfied (Fig. 1A)

$$E_Z > \sqrt{\Delta^2 + \mu^2} \qquad (1)$$

where $E_Z = g\mu_B B$ is the Zeeman energy, with g as the effective Landé g factor and μ_B as the Bohr magneton. Δ is the induced superconducting

gap at $B = 0$, and μ is the chemical potential in the quantum wire, with $\mu = 0$ set to coincide with the lowest energy of a one-dimensional subband at $B = 0$. Equation 1 defines the topological superconducting phase in a clean and infinite system. In a real nanowire device, the phase boundary is transformed because of electron-electron interactions (7), magnetic vector potential (8), as well as finite size effects and disorder (9–13).

We test Eq. 1 in a device built around an InSb semiconductor nanowire with an NbTiN contact used to induce superconductivity and a normal metal Pd contact used to perform tunneling spectroscopy by varying the bias voltage V between normal and superconducting contacts (Fig. 1B) (see the Supplementary Materials). To identify MBS, we look for conductance peaks at zero source-drain voltage bias (16, 17). Both magnitude and direction of field B can be controlled because B should be pointed away from the direction of the effective spin-orbit field to induce MBS. We find ZBPs consistent with MBS for fields below 1 T. The induced superconducting gap Δ at zero field is set by the NbTiN/InSb interface transparency and by the electronic band structure in the nanowire. A nanowire fully covered by a superconductor can exhibit a hard induced gap (see the Supplementary Materials) (18, 19). However, to enable gate tuning of the chemical potential μ under the superconductor in the range sufficient for exploring the phase diagram, the nanowire is designed to be partially covered with a superconductor, resulting in a "soft" gap (16, 20).

We adjust the voltage on gate FG1 to create a tunneling barrier between normal and superconducting sides. Gate BG1, located next to the tunneling barrier and underneath the superconductor, is used to vary the chemical potential in the nanowire segment under investigation.

We first demonstrate the ability to generate or eliminate a ZBP in conductance over a wide range of B by switching the voltage on gate BG1. Figure 1 (C to E) presents scans of bias voltage versus the magnetic field applied along the nanowire at three different BG1 voltages. The scan obtained at BG1 = −0.42 V (Fig. 1D) shows a ZBP persistent in the magnetic field from $B = 0.4$ to 1 T. When BG1 is changed by ±0.11 V (Fig. 1, C and E), no ZBPs appear up to 1 T, and only a gradual closing of the induced gap is observed. Thus, Fig. 1 (C to E) constrains the ZBP phase diagram (horizontal lines in Fig. 1A). Magnetic field sweeps taken with a fine step in BG1 gate voltage reveal further details of the ZBP evolution, including a gate-tunable onset, deviations from zero bias, and peak splitting (see the Supplementary Materials). It is noteworthy that the ZBP shows no significant dependence on other gates (FG2, BG2, and BG3), which indicates that ZBP is from quantum states located in the nanowire above BG1 (see the Supplementary Materials).

[1]Department of Physics and Astronomy, University of Pittsburgh, Pittsburgh, PA 15260, USA. [2]Department of Physics and Astronomy, West Virginia University, Morgantown, WV 26506, USA. [3]Institut Néel, CNRS, 38042 Grenoble, France. [4]Eindhoven University of Technology, 5600 MB Eindhoven, Netherlands. [5]Centre National de la Recherche Scientifique, LAAS, Université de Toulouse, 31031 Toulouse, France. [6]QuTech and Kavli Institute of Nanoscience, Delft University of Technology, 2628 CJ Delft, Netherlands.
*These authors contributed equally to this work.
†Present address: Department of Electrical and Computer Engineering, University of Pittsburgh, Pittsburgh, PA 15261, USA.
‡Present address: Condensed Matter Theory Center and Joint Quantum Institute, Department of Physics, University of Maryland, College Park, MD 20742–4111, USA.
§Corresponding author. Email: frolovsm@pitt.edu

In Fig. 2, we present the emergence and the evolution of the ZBP within the phase space identified in Fig. 1. At zero field, a bias versus gate scan exhibits an induced gap $\Delta = 0.25$ meV (Fig. 2A). We assign the conductance maxima at $V = \pm0.25$ mV and around BG1 = −0.4 V to an increase in the density of states at the bottom

of the second one-dimensional subband (see the Supplementary Materials for discussion). At $B = 0.25$ T (Fig. 2B), the apparent gap decreases, but the regime remains qualitatively similar to that at $B = 0$ T. We point out that all bias versus gate data from this device is asymmetric in bias. That is, resonances that shift to a more
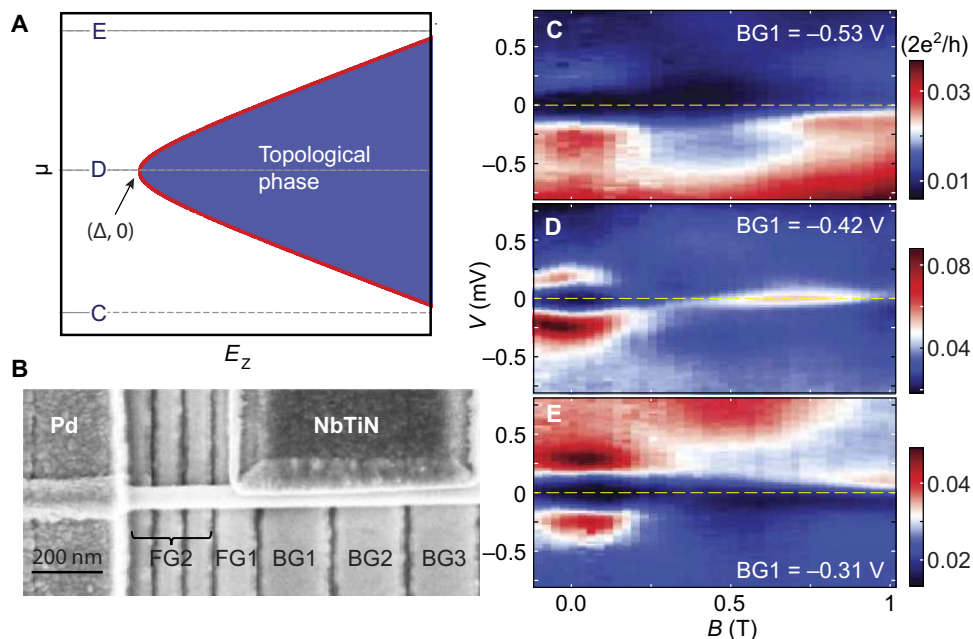

Fig. 1. ZBP in a nanowire device controlled by gate voltages. (A) Topological phase diagram described by Eq. 1. Dashed lines indicate settings of μ in (E), (D), and (C). **(B)** Scanning electron micrograph of the device used in this work. An InSb nanowire is half-covered by a superconductor NbTiN and normal metal Pd contact. The nanowire is placed on FG and BG metal gates. **(C to E)** Differential conductance maps in bias voltage V versus magnetic field B at three different settings of BG1.
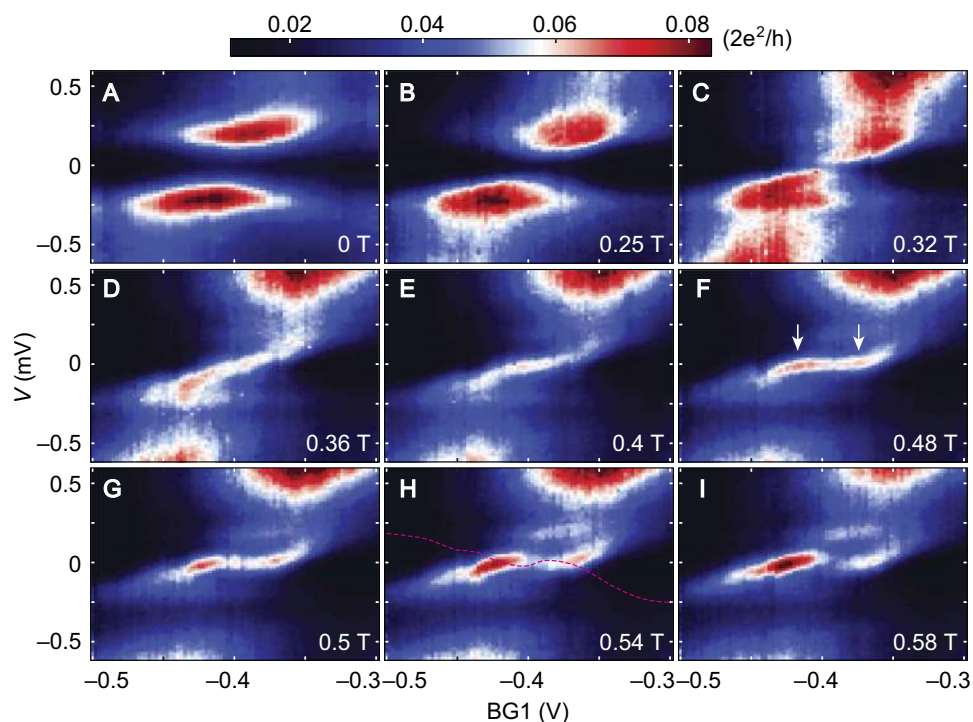

Fig. 2. The emergence of the ZBP. (A to I) Conductance maps in bias voltage V versus BG1 at different magnetic fields indicated in the lower right corner of each panel. The arrows in (F) mark the ZBP onset gate voltages plotted in Fig. 3. The dashed line in (H) is obtained by tracing the visible maximum in subgap conductance and flipping the resulting trace around $V = 0$ mV.

positive bias voltage with a more positive gate voltage dominate. This behavior is characteristic for finite-size superconducting systems with highly asymmetric barriers (*21*).

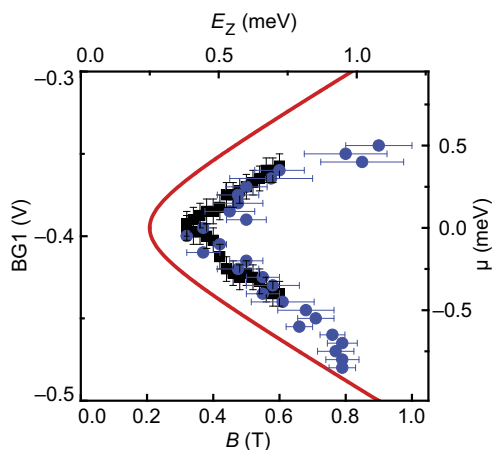At $B = 0.32$ T (Fig. 2C), the conductance within the induced gap is increased in the center of the BG1 range, giving an indication of a closing gap at BG1 = −0.4 V. According to the theory behind Eq. 1, the gap should close around μ = 0 at the topological phase transition. At $B = 0.36$ T, a well-defined conductance resonance crosses zero bias and extends across the gap (Fig. 2D). The resonance appears to stick to zero bias in a widening range of BG1 at higher magnetic fields (Fig. 2, E and F). Toward the edges of each BG1 scan, the conductance peak strongly deviates from zero bias and gradually merges into the apparent induced gap. At the boundary defined by Eq. 1, MBSs at the opposite ends of the topological segment of the nanowire grow in length and strongly overlap because of the finite length of the segment. This overlap of the two MBSs leads to the MBS energy deviating from zero (*12*, *22–25*).

In addition to the strong deviations from zero bias at the phase boundaries, we observe that for $B \geq 0.5$ T (Fig. 2, G to I), the peak wavers away from zero bias near the center of the scans. Particle-hole symmetry in the superconductor dictates that the energy spectrum within the gap must be symmetric with respect to zero bias. This is not observed because of barrier asymmetry (*21*). However, to propose how the full spectrum inside the gap looks, we trace a subgap resonance in Fig. 2H and flip it along the zero bias line. The full spectrum obtained this way suggests that the small deviations from zero bias also originate from ZBP splitting due to gate-dependent overlap of MBSs within the topological phase. These deviations from zero bias are also observed in detailed field sweeps presented in the Supplementary Materials.

We map out the phase diagram of ZBPs: From the extended data set represented in Fig. 2 and from fig. S4, we pick the onset points of ZBPs in gate BG1 and in the magnetic field and plot them in Fig. 3. The two data sets obtained this way are consistent with the square root dependence predicted by Eq. 1. On the basis of the diagram, we identify μ = 0 at BG1 = −0.4 V. The minimal onset field $B = 0.33$ T converts

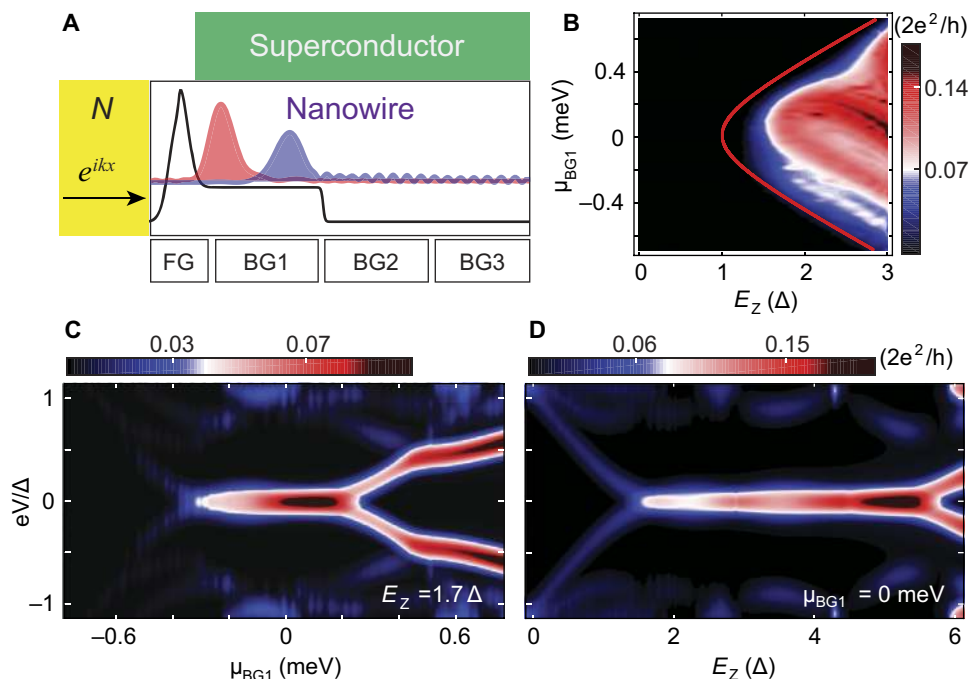**Fig. 3. Phase diagram of ZBPs.** ZBP onset points are collected from the extended data set represented in Fig. 2 (black squares) and from fig. S4 (blue circles), with error bars judged by deviation of the peak from zero bias within one-half of the full width at half maximum of ZBPs. Data extracted from fig. S4 are offset by +0.02 V in BG1 to compensate for a systematic shift due to a charge switch. The top axis E_Z is calculated from the magnetic field using $g = 40$. The right axis μ is calculated from BG1 according to 10 meV/V (see fig. S8A in the Supplementary Materials) and set to zero at the parabolic vertex, BG1 = −0.395 V. Equation 1 is plotted in solid line using Δ = 0.25 mV.

Fig. 4. Tight-binding model results reveal two weakly coupled MBSs. (**A**) Model schematics. A nanowire is contacted by a superconductor and a normal metal. The potential profile is shown as the black curve. A plane wave e^{ikx} coming from *N* can tunnel into the nanowire through the barrier above FG. The chemical potential above BG1, μ_{BG1}, is tunable, whereas potentials above BG2 and BG3 are fixed. The calculated wave function amplitudes for zero-energy states are shown in red and blue. (**B**) Conductance map taken at zero bias. The red curve corresponds to a plot of Eq. 1. (**C**) Conductance map in bias energy versus chemical potential at $E_Z = 1.7$ Δ. (**D**) Conductance map in bias energy versus Zeeman energy splitting at $\mu_{BG1} = 0$ meV. In (B) to (D), thermal broadening is set to 50 μeV to match the experimental ZBP width.

into Zeeman energy of 0.4 meV (using $g = 40$), which is greater than the apparent gap at $B = 0$ T. Actually, in finite length superconductors, the following is expected: Because of MBS splitting at the topological transition point, the ZBP should onset at a higher field. For the same reason, a ZBP should appear in a narrower range of chemical potential around $\mu = 0$ for a fixed field. As a result, the area of the phase with ZBP present is reduced for finite-size systems. In Fig. 3, the theoretical phase transition line predicted by Eq. 1 encircles the extracted ZBP onset points.

The resonance that we investigate as MBS is pinned near zero bias over a significant phase diagram area (see the Supplementary Materials). The range of ZBP in both chemical potential and Zeeman energy greatly exceeds the ZBP width, which is between 30 and 100 μeV. The phase diagram area with a ZBP is strongly diminished when magnetic field orientation deviates from the nanowire main axis and approaches the spin-orbit field orientation, previously established as perpendicular to the nanowire (see the Supplementary Materials) (16, 26, 27).

The similarities between trivial Andreev and Majorana states currently represent the greatest challenge of the tunneling technique (28–30). We present Andreev bound states observed in the same device at different gate settings in the Supplementary Materials. Trivial Andreev states intermittently cross zero bias and yield a similar phase boundary to that in Fig. 3. In this case, the phase boundary separates even and odd parity ground states. However, Andreev resonances cross zero bias over a narrow range of field and gate voltage in the immediate vicinity of the boundary, leaving the conductance near zero bias low within the boundary at distances exceeding the conductance peak width in bias.

Next, we set up a quasi–one-dimensional tight-binding model to numerically study a finite-length nanowire under the conditions set by Eq. 1. To match the experimental conditions, we created a high potential barrier above FG; the potential above BG1, μ_{BG1}, is continuously tuned, whereas the potential above BG2 and BG3 is kept constant (Fig. 4A). Figure 4A also shows calculated wave function amplitude profiles of the two MBSs. The left MBS decays into the barrier region above FG. The right MBS has an evanescent tail, which extends to nontopological regions above BG2 and BG3. These tails are responsible for a reduced overlap between left and right MBSs. Because of the small MBS overlap, the oscillations of the MBS do not reach large amplitudes in energy. The conductance map at zero bias in chemical potential versus Zeeman energy is calculated from the tunneling rates of quantum states (Fig. 4B). The boundary of the increased zero-bias conductance region is consistent with the experimental data in Fig. 3 and fig. S8, where the minimum onset field of ZBP is also observed to be larger than $E_Z = \Delta$. The conductance oscillations inside the high conductance region are due to MBS oscillations.

If thermal broadening is included, conductance resonances appear as a single ZBP despite MBS oscillations. In Fig. 4C, at a finite Zeeman splitting of 1.7 Δ, we observe an extended ZBP at the center of the map. The zero-bias state occupies a similar range of chemical potential as in the experimental conductance map in Fig. 2F, except that both branches of the spectrum are visible in the simulation. Conductance is suppressed at more negative values of the chemical potential because the states move farther from the probe lead N. In the conductance map at chemical potential $\mu_{BG1} = 0$ meV (Fig. 4D), an extended ZBP is present from $E_Z = 1.5$ up to 5.8 Δ. See the Supplementary Materials for calculation details.

Comparison between the model (Fig. 4, B to D) and the experiment (Figs. 1 to 3) allows us to conclude that ZBP occurs in the parameter region that is consistent with the predicted topological superconducting phase for a finite-size nanowire segment. According to the model, the two MBSs are separated by a distance of the same order as the coherence length. Further evidence of topological superconductivity can be obtained in longer topological segments (31–33), which can be achieved through further improvements in gate design and superconductor-semiconductor interface preparation (18, 19, 22).

MATERIALS AND METHODS

InSb nanowires were grown by Au-catalyzed vapor-liquid-solid mechanism in a metalorganic vapor phase epitaxy reactor. Nanowires were deposited onto bottom gate chips using a micromanipulator. Nanowires have diameters ranging from 60 to 100 nm. The bottom gates are made of Ti (5 nm)/Au (10 nm), with FG gates 50/100 nm wide and BG gates 200 nm wide. A layer of high-κ dielectric HfO$_2$ (10 nm) was deposited onto the bottom gates. Before contact deposition, the nanowire was processed in a 1:500 diluted ammonium sulfide solution by baking for 30 min at 55°C to remove a native oxide layer.

The superconducting contact is a trilayer of Ti (5 nm)/NbTi (5 nm)/NbTiN (180 nm) optimized to suppress subgap conductance. The normal contact is a Ti (15 nm)/Pd (150 nm) stack; before its deposition, a gentle argon plasma cleaning was performed in situ.

Measurements were performed in a dilution refrigerator at a base temperature of 30 mK by standard low-frequency lock-in technique (77.77 Hz, 5 μV). Multiple stages of filtering were used to enhance the signal-to-noise ratio. For all the measurements, bias voltage was applied to the normal contact, and the superconducting contact was grounded.

SUPPLEMENTARY MATERIALS

Supplementary material for this article is available at http://advances.sciencemag.org/cgi/content/full/3/9/e1701476/DC1

Supplementary Text
fig. S1. Hard gap in a double full-cover superconducting device.
fig. S2. Linecuts from Figs. 1 and 2 in the main text.
fig. S3. Gates dependence of ZBP.
fig. S4. ZBP evolution with BG1.
fig. S5. ZBP evolution at a large range of magnetic field.
fig. S6. Magnetic field orientation dependence of ZBP.
fig. S7. ZBP evolution with BG1 at an angle of π/2.
fig. S8. Expanded scan of BG1 and gates dependence of resonances.
fig. S9. Comparing the first and second resonances in zero-bias conductance maps.
fig. S10. Gate and field dependence of the second resonance.
fig. S11. Schematic representation of the tight-binding Hamiltonian.
fig. S12. Comparison between long and short wires on spatial and Zeeman-field dependence of the lowest-energy states.
fig. S13. Low-energy spectrum and corresponding conductance map at different Zeeman fields.
fig. S14. Low-energy spectrum and corresponding conductance map for a system with a step-like potential.
fig. S15. Differential conductance at high values of μ_{BG1}.
fig. S16. Conductance and local-density maps of particle states at zero field.
fig. S17. Conductance maps for different potential profiles.
fig. S18. Conductance map of bias versus μ_{BG1} and corresponding potential profile for different BG2 settings.
References (34–37)

REFERENCES AND NOTES

1. A. Y. Kitaev, Unpaired Majorana fermions in quantum wires. Phys. Usp. **44**, 131–136 (2001).
2. N. Read, D. Green, Paired states of fermions in two dimensions with breaking of parity and time-reversal symmetries and the fractional quantum hall effect. Phys. Rev. B **61**, 10267 (2000).

3. A. Y. Kitaev, Fault-tolerant quantum computation by anyons. *Ann. Phys.* **303**, 2–30 (2003).

4. C. Nayak, S. H. Simon, A. Stern, M. Freedman, S. Das Sarma, Non-Abelian anyons and topological quantum computation. *Rev. Mod. Phys.* **80**, 1083–1159 (2008).

5. J. Alicea, Y. Oreg, G. Refael, F. von Oppen, M. P. A. Fisher, Non-Abelian statistics and topological quantum information processing in 1d wire networks. *Nat. Phys.* **7**, 412–417 (2011).

6. B. van Heck, A. R. Akhmerov, F. Hassler, M. Burrello, C. W. J. Beenakker, Coulomb-assisted braiding of Majorana fermions in a Josephson junction array. *New J. Phys.* **14**, 035019 (2012).

7. E. M. Stoudenmire, J. Alicea, O. A. Starykh, M. P. A. Fisher, Interaction effects in topological superconducting wires supporting Majorana fermions. *Phys. Rev. B* **84**, 014503 (2011).

8. B. Nijholt, A. R. Akhmerov, Orbital effect of magnetic field on the Majorana phase diagram. *Phys. Rev. B* **93**, 235434 (2015).

9. A. Vuik, D. Eeltink, A. R. Akhmerov, M. Wimmer, Effects of the electrostatic environment on the Majorana nanowire devices. *New J. Phys.* **18**, 033013 (2016).

10. İ. Adagideli, M. Wimmer, A. Teker, Effects of electron scattering on the topological properties of nanowires: Majorana fermions from disorder and superlattices. *Phys. Rev. B* **89**, 144506 (2014).

11. A. C. Potter, P. A. Lee, Majorana end states in multiband microstructures with Rashba spin-orbit coupling. *Phys. Rev. B* **83**, 094525 (2011).

12. T. D. Stanescu, R. M. Lutchyn, S. Das Sarma, Dimensional crossover in spin-orbit-coupled semiconductor nanowires with induced superconducting pairing. *Phys. Rev. B* **87**, 094518 (2013).

13. A. M. Lobos, S. Das Sarma, Tunneling transport in NSN Majorana junctions across the topological quantum phase transition. *New J. Phys.* **17**, 065010 (2015).

14. R. M. Lutchyn, J. D. Sau, S. Das Sarma, Majorana fermions and a topological phase transition in semiconductor-superconductor heterostructures. *Phys. Rev. Lett.* **105**, 077001 (2010).

15. Y. Oreg, G. Refael, F. von Oppen, Helical liquids and Majorana bound states in quantum wires. *Phys. Rev. Lett.* **105**, 177002 (2010).

16. V. Mourik, K. Zuo, S. M. Frolov, S. Plissard, E. P. A. M. Bakkers, L. P. Kouwenhoven, Signatures of Majorana fermions in hybrid superconductor-semiconductor nanowire devices. *Science* **336**, 1003–1007 (2012).

17. S. Nadj-Perge, I. K. Drozdov, J. Li, H. Chen, S. Jeon, J. Seo, A. H. MacDonald, B. A. Bernevig, A. Yazdani, Observation of Majorana fermions in ferromagnetic atomic chains on a superconductor. *Science* **346**, 602–607 (2014).

18. H. Zhang, Ö. Gül, S. Conesa-Boj, K. Zuo, V. Mourik, F. K. de Vries, J. van Veen, D. J. van Woerkom, M. P. Nowak, M. Wimmer, D. Car, S. Plissard, E. P. A. M. Bakkers, M. Quintero-Pérez, S. Goswami, K. Watanabe, T. Taniguchi, L. P. Kouwenhoven, Ballistic superconductivity in semiconductor nanowires. *Nat. Commun.* **8**, 16025 (2017).

19. W. Chang, S. M. Albrecht, T. S. Jespersen, F. Kuemmeth, P. Krogstrup, J. Nygård, C. M. Marcus, Hard gap in epitaxial semiconductorsuperconductor nanowires. *Nat. Nanotechnol.* **10**, 232–236 (2015).

20. T. D. Stanescu, R. M. Lutchyn, S. Das Sarma, Soft superconducting gap in semiconductor-based Majorana nanowires. *Phys. Rev. B* **90**, 085302 (2014).

21. J. Stenger, T. D. Stanescu, Tunneling conductance in semiconductor-superconductor hybrid structures. https://arxiv.org/abs/1703.02543 (2017).

22. S. M. Albrecht, A. P. Higginbotham, M. Madsen, F. Kuemmeth, T. S. Jespersen, J. Nygård, P. Krogstrup, C. M. Marcus, Exponential protection of zero modes in Majorana islands. *Nature* **531**, 206–209 (2016).

23. E. Prada, P. San-Jose, R. Aguado, Transport spectroscopy of NS nanowire junctions with Majorana fermions. *Phys. Rev. B* **86**, 180503 (2012).

24. S. Das Sarma, J. D. Sau, T. D. Stanescu, Splitting of the zero-bias conductance peak as smoking gun evidence for the existence of the Majorana mode in a superconductor-semiconductor nanowire. *Phys. Rev. B* **86**, 220506 (2012).

25. D. Rainis, L. Trifunovic, J. Klinovaja, D. Loss, Towards a realistic transport modeling in a superconducting nanowire with Majorana fermions. *Phys. Rev. B* **87**, 024515 (2013).

26. S. Nadj-Perge, V. S. Pribiag, J. W. G. van den Berg, K. Zuo, S. R. Plissard, E. P. A. M. Bakkers, S. M. Frolov, L. P. Kouwenhoven, Spectroscopy of spin-orbit quantum bits in indium antimonide nanowires. *Phys. Rev. Lett.* **108**, 166801 (2012).

27. C.-H. Lin, J. D. Sau, S. Das Sarma, Zero-bias conductance peak in Majorana wires made of semiconductor/superconductor hybrid structures. *Phys. Rev. B* **86**, 224511 (2012).

28. A. Das, Y. Ronen, Y. Most, Y. Oreg, M. Heiblum, H. Shtrikman, Zero-bias peaks and splitting in an Al–InAs nanowire topological superconductor as a signature of Majorana fermions. *Nat. Phys.* **8**, 887–895 (2012).

29. E. J. H. Lee, X. Jiang, M. Houzet, R. Aguado, C. M. Lieber, S. De Franceschi, Spin-resolved Andreev levels and parity crossings in hybrid superconductor–semiconductor nanostructures. *Nat. Nanotechnol.* **9**, 79–84 (2014).

30. M. T. Deng, S. Vaitiekenas, E. B. Hansen, J. Danon, M. Leijnse, K. Flensberg, J. Nygård, P. Krogstrup, C. M. Marcus, Majorana bound state in a coupled quantum-dot hybrid-nanowire system. *Science* **354**, 1557–1562 (2016).

31. L. Fu, Electron teleportation via Majorana bound states in a mesoscopic superconductor. *Phys. Rev. Lett.* **104**, 056402 (2010).

32. B. van Heck, F. Hassler, A. R. Akhmerov, C. W. J. Beenakker, Coulomb stability of the 4π-periodic Josephson effect of Majorana fermions. *Phys. Rev. B* **84**, 180502 (2011).

33. D. Aasen, M. Hell, R. V. Mishmash, A. Higginbotham, J. Danon, M. Leijnse, T. S. Jespersen, J. A. Folk, C. M. Marcus, K. Flensberg, J. Alicea, Milestones toward Majorana-based quantum computing. *Phys. Rev. X* **6**, 031016 (2016).

34. I. van Weperen, S. R. Plissard, E. P. A. M. Bakkers, S. M. Frolov, L. P. Kouwenhoven, Quantized conductance in an InSb nanowire. *Nano Lett.* **13**, 387–391 (2013).

35. J. Kammhuber, M. C. Cassidy, H. Zhang, Ö. Gül, F. Pei, M. W. A. de Moor, B. Nijholt, K. Watanabe, T. Taniguchi, D. Car, S. R. Plissard, E. P. A. M. Bakkers, L. P. Kouwenhoven, Conductance quantization at zero magnetic field in InSb nanowires. *Nano Lett.* **16**, 3482–3486 (2016).

36. I. van Weperen, B. Tarasinski, D. Eeltink, V. S. Pribiag, S. R. Plissard, E. P. A. M. Bakkers, L. P. Kouwenhoven, M. Wimmer, Spin-orbit interaction in InSb nanowires. *Phys. Rev. B* **91**, 201413 (2015).

37. G. E. Blonder, M. Tinkham, T. M. Klapwijk, Transition from metallic to tunneling regimes in superconducting microconstrictions: Excess current, charge imbalance, and supercurrent conversion. *Phys. Rev. B* **25**, 4515–4532 (1982).

Citation: J. Chen, P. Yu, J. Stenger, M. Hocevar, D. Car, S. R. Plissard, E. P. A. M. Bakkers, T. D. Stanescu, S. M. Frolov, Experimental phase diagram of zero-bias conductance peaks in superconductor/semiconductor nanowire devices. *Sci. Adv.* **3**, e1701476 (2017).

Science Advances

Experimental phase diagram of zero-bias conductance peaks in superconductor/semiconductor nanowire devices

Jun Chen, Peng Yu, John Stenger, Moïra Hocevar, Diana Car, Sébastien R. Plissard, Erik P. A. M. Bakkers, Tudor D. Stanescu and Sergey M. Frolov

ARTICLE TOOLS	http://advances.sciencemag.org/content/3/9/e1701476
SUPPLEMENTARY MATERIALS	http://advances.sciencemag.org/content/suppl/2017/09/01/3.9.e1701476.DC1
REFERENCES	This article cites 36 articles, 3 of which you can access for free http://advances.sciencemag.org/content/3/9/e1701476#BIBL
PERMISSIONS	http://www.sciencemag.org/help/reprints-and-permissions

Use of this article is subject to the Terms of Service